



# Relative amplitude preservation in high-resolution shallow reflection seismic: a case study from Fore-Sudetic Monocline, Poland

K. Cichostępski<sup>1</sup> · J. Dec<sup>1</sup> · A. Kwietniak<sup>1</sup>

Received: 31 July 2018 / Accepted: 23 December 2018 / Published online: 19 January 2019  
© The Author(s) 2019

## Abstract

The acquisition parameters and methodology of seismic data processing for high-resolution seismic imaging viewed through relative amplitude preservation are presented. An example of the obtaining of high-quality, shallow seismic data with a variable end-on spread is shown. The source used for the project is an accelerated weight drop. The study area lies within the mine waste disposal area, near Rudna village (Fore-Sudetic Monocline, WS Poland), and results are given for a 2D experimental profile. The aim of the project was to design optimal acquisition and processing parameters for the detailed recognition of Tertiary deposits. The proposed acquisition parameters are a compromise between time, cost and results. High-resolution seismic imaging enables the determining of layers within the range of thicknesses between 5 and 15 m, while the maximal depth of imaging reaches 400 m.

**Keywords** High-resolution seismic · Thin layers · Acquisition · Weight drop · Noise attenuation · Relative amplitude processing

## Introduction

Throughout the last 30 years, the interest in engineering and environmental applications of seismic methods for high-resolution imaging of the near surface has increased intensively. Scientists have come to realize that high-resolution imaging is key to understanding the complex nature of many geological targets better (e.g. Berkhout 1985; Sheriff 1985, 1997).

Exploration geophysics is focused on structural and reservoir depth range. It can reach up to several kilometers, registering frequency band spans comprising several tens of Hertz, although the dominant frequency is typically below 50 Hz, depending on the source parameters and the target depth. In contrast to deep seismic imaging, shallow seismic uses sources of significantly lower energies but with a much higher frequency range, guaranteeing higher resolution of data. Higher frequencies are attenuated more efficiently, however, limiting the depth range of such a signal. The application of near-surface seismic imaging is used mainly

for engineering purposes (Steeple and Miller 1990), recognition of shallow geological structures, e.g., depositional sequences (Baumgart-Kotarba et al. 2001), subglacial structures (Benjumea and Teixido 2001), post-glacial deposits (Francese et al. 2007; Baumgart-Kotarba et al. 2008), fault zones (Myers et al. 1987; Treadway et al. 1988; Miller et al. 1989, 1990) and shallow exploration targets, for example zinc ore (Singh 1984), sulfur ore deposits (Dec 2012; Dec and Cichostępski 2017a, b) and coal beds (Palmer 1987).

The idea of applying high-frequency sources to shallow seismic exploration has been discussed for many years (e.g. Knapp and Steeples 1986b). The comparison of different sources can be found in many research papers, for example, Miller et al. (1986, 1992, 1994) or Atanackov and Gosar (2013), an interesting comparison of seismic sources can be found presented by Miller et al. (1986)—concerning piezoelectric sources, hammering, weight dropping, rifle shot and others actions. The signals obtained have very wide frequency bands and dominant frequencies of 120–200 Hz. The depth range presented by the authors reaches approximately 200 ms. Similar results are presented by Steeples and Miller (1990) where the depth ranges are within 200–300 ms. A particularly interesting idea was the application of a .5 caliber rifle shot and vertical stacking that enabled the reaching of high-frequency data for a depth range of up to

✉ K. Cichostępski  
kcichy@agh.edu.pl

<sup>1</sup> Faculty of Geology, Geophysics and Environmental Protection, AGH-UST University of Science and Technology, Kraków, Poland

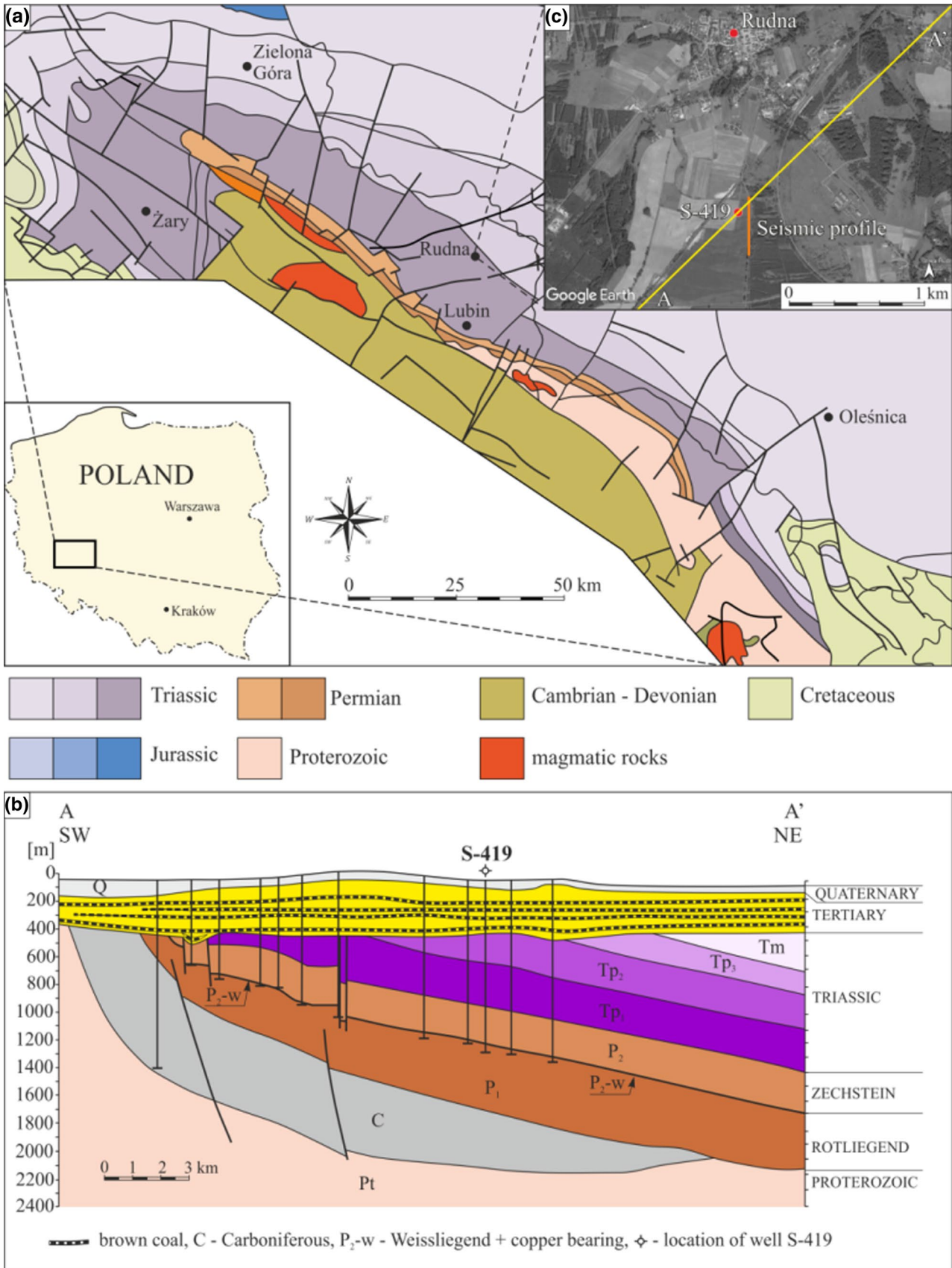


**Fig. 1** Localization of study area. **a** Geological map of Fore-Sudetic Monocline without Cenozoic (after Pożaryski 1979, modified); **b** geological profile A–A' across study area (after Kłapciński et al. 1984, modified); **c** location of experimental seismic profile (orange), geological profile A–A' (yellow) and wellbore S-419 (source of map: Google Earth)

1000 m (Steeple and Miller 1990). Nevertheless, the explosive sources, such as rifle or sparker, requires the drilling of shallow wells (holes) that are filled with water for which permission should be issued by the local authorities. This increases the costs and extends the time needed for seismic acquisition.

In shallow seismic, weight-based sources are common and the acquisition parameters (live channels, offset range, fold) are proportionally smaller than in large-scale exploration seismic surveys. The problem of overriding importance in shallow seismic imaging is the maintaining of the widest frequency bands with a low noise content—high signal-to-noise ratio (S/N ratio). Very low fold value governs the need for adjusting an appropriate acquisition design, taking into account geometry, source and receiver parameters and processing sequences for the specific target. A low fold parameter also causes a resolution enhancement at the processing step, which must often be compensated for by a significant alteration of seismic wavelet. This enhancement is highly undesirable—every arbitral change of a seismic wavelet results in a false reservoir interpretation and should be omitted at all costs. In the case of imaging shallow exploration targets and lithofacial analysis, it is crucial not to disturb the relative amplitude ratios which are almost impossible to interpret when a seismic wavelet is distorted. Petrophysical parameter determination relies on amplitude value and its changes (Dec and Cichostępski 2017a, b; Kwietniak et al. 2018), so it is highly necessary to keep seismic with relative amplitude preservation (RAP) versions for such purposes.

RAP, originally defined as reflection amplitude preservation (Sheriff 1991), is “processing and display designed to preserve relative amplitudes of seismic reflections.” It was a Western Geophysical trademark, later to be used generally as a name for seismic volumes that underwent no amplitude changes. RAP-processed sections enable linking amplitude changes with lateral and vertical changes in petrophysical properties of a geological medium. Only such a volume can be treated as input data to any reservoir (petrophysical) analyses, such as the inversion process, AVO analysis or instantaneous attribute application. The processing criteria for relative amplitude preservation were stipulated by Shuey (1985).

RAP, altogether with the need for high-resolution data, was a key factor in our research. In comparison with the previously mentioned results (Steeple and Miller 1990), the dominant frequency is lower, around 125 Hz, but the result

can still be considered as high-resolution seismic data. This was the result of an accurate choice of the sensors used and the processing algorithms. In the following paper, we would like to present the methodology that was a tradeoff between result quality and all other costs behind the seismic acquisition. Our approach can easily be applied in similar geological settings.

Currently, RAP processing is the standard approach in exploration seismology. It is rarely applied in near-surface studies. We want to show that this kind of restricted processing can be also exploited in high-resolution shallow seismic investigation. RAP-processed high-resolution shallow seismic data can be used further for the imaging of petrophysical parameters distribution, in the near-surface zone.

### Location and geological setting

The survey area is located within the Fore-Sudetic Monocline in SW Poland, near Rudna village and in proximity to copper and silver mine ‘Rudna’ (property of KGHM Concern). The scope of the research project was to determine the morphology and characteristics of Tertiary sediments to find the optimal location for seismograms of the European Plate Observing System (EPOS). The location of the experimental 2D seismic profile is shown in Fig. 1.

The geological sequence within the study area consists of Proterozoic, Carboniferous, Permian (Lower Permian—Rotliegend formation and Upper Permian—Zechstein), Triassic, Tertiary (Palaeogene and Neogene) and Quarterly (Kłapciński et al. 1984).

The Triassic is represented by the complete profile of Lower Triassic sandstones—Roethian (Olenekian and Induan). The Lowermost Triassic is built from arkosic and quartzitic sandstones; the thickness of these deposits is about 300 m. The Middle Bundsandstein (Middle Lower Triassic) is comprised of arkosic sandstones with a band of brown and dark gray shales. Dolomites and marls represent Ret with platies of limestones and anhydrite. The thickness of Ret reaches up to 140 m.

Uppermost in the profile lays Palaeogene (Eocene and Oligocene) and Neogene (Miocene and Pliocene). The Eocene consists of quartz-rich and glauconite sandstones with thicknesses of 20 m. The Oligocene is represented by similar lithologies with a small admixture of gravel of thicknesses of 20 m. Brown coal beds—the Głogowski beds—closes the Paleogene profile. The Miocene profile consists of gravels, quartz sands and green and gray argil. Within the Miocene sediments, there are three brown coal beds: Ścinawski, Łużycki and Henryk coal beds (Kłapciński and Peryt 2007). Toward the top of the profile, above the Henryk coal bed, there are argillitic Pliocene sediments, which have an interlining of quartz sandstones. The thickness of the Pliocene deposits is locally less than 100 m.

The Quaternary sediments have thicknesses of several tens of meters. They consist of post-glacial deposits, mostly rich in quartz sandstones, gravels and gray clays. Within the gray clays, additives of sands and gravel beds can often be encountered.

Within the Tertiary sediments, thin bed sequences of sandstone and argil, as well as brown coal beds, are common. The tops and beds of the coal layers are very strong reflective boundaries, thus producing a rapid decrease in energy (attenuation) carried by the elastic field through the deeper intervals, causing a decreased resolution of seismic image below the coal bed sequences.

In some places, the complex glaciotectionic processes have caused the Pliocene illites to be overthrust into the Quaternary sediments also causing difficulties in structural interpretation. Adding to the fact that the Quaternary sediments are rather loose, which also results in substantial attenuation of a seismic signal, the whole geological interval under analysis requires a well thought out acquisition design and processing approach.

### Field test of geophones

A common practice in reflection seismic imaging is to use geophones of natural frequencies between 10 and 25 Hz. With well-defined source parameters (i.e., vibroseis sweep, dynamite), 14-Hz geophones are used. Before proceeding with the acquisition, we decided to compare the results and spectral characteristics of seismic records obtained by 14-Hz and 100-Hz geophones. The comparison of the normalized geophone responses of these two is presented in Fig. 2.

The 14-Hz geophones have flat frequency characteristic from 80 Hz, but maximal amplitude frequency (dominant

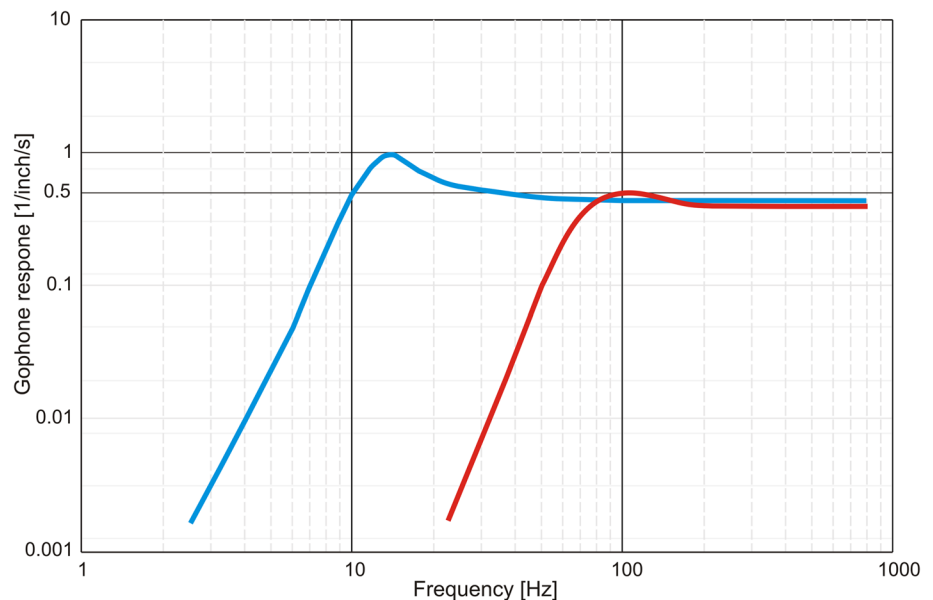
frequency) lies within 8–30 Hz. The usage of 14-Hz geophones results in increased dynamics of low-frequency components and consequently higher detectability and visibility of surface wave. The 100-Hz geophones attenuate much more efficiently the low frequencies that cause the surface wave and other low-frequency noise, producing less dominance on the field record. For the same velocity of displacement the shape of the frequency response above 100 Hz is similar, but in bandwidth between 8 and 80 Hz, the response from 14 Hz sensors has much higher amplitudes. To verify these characteristics, the field test of two sets of sensors was conducted.

The field test was performed on the same line with the same geometry for 14 Hz and 100 Hz sensors. The source used was ESS-500 Turbo (Gisco), located at the same place for both recordings. (To keep the source characteristic similar, the shot point position was firmed.) The source is an accelerating weight of 227 kg (an accelerated drop using an elastic rubber band; impact velocity is of 3 m/s with an energy of  $E = 1022$  J). The results obtained by the two sets of sensors are presented in Fig. 3.

The test results show that in the case of 100-Hz geophones, amplitudes for frequencies 0–50 Hz are much attenuated and the spectrum amplitudes within a bandwidth of 50–200 Hz are highly favorable (Fig. 3b). The  $-12$  dB bandwidth equals 120 Hz (40–160 Hz). The  $-6$  dB bandwidth registered by 100-Hz geophones is between 60 and 130 Hz (Fig. 3b), and for 14 Hz it is between 30 and 80 Hz (Fig. 3a).

Frequency spectra show that the signal generated by ESS-500 Turbo has a broad frequency characteristic. Between frequencies of 100–200 Hz, the amplitude values are significant and the application of deconvolution should result in a wide and flat spectrum. According to Knapp and Steeples

**Fig. 2** Normalized geophone responses: blue line—14 Hz, red line—100 Hz (Gisco 2018)



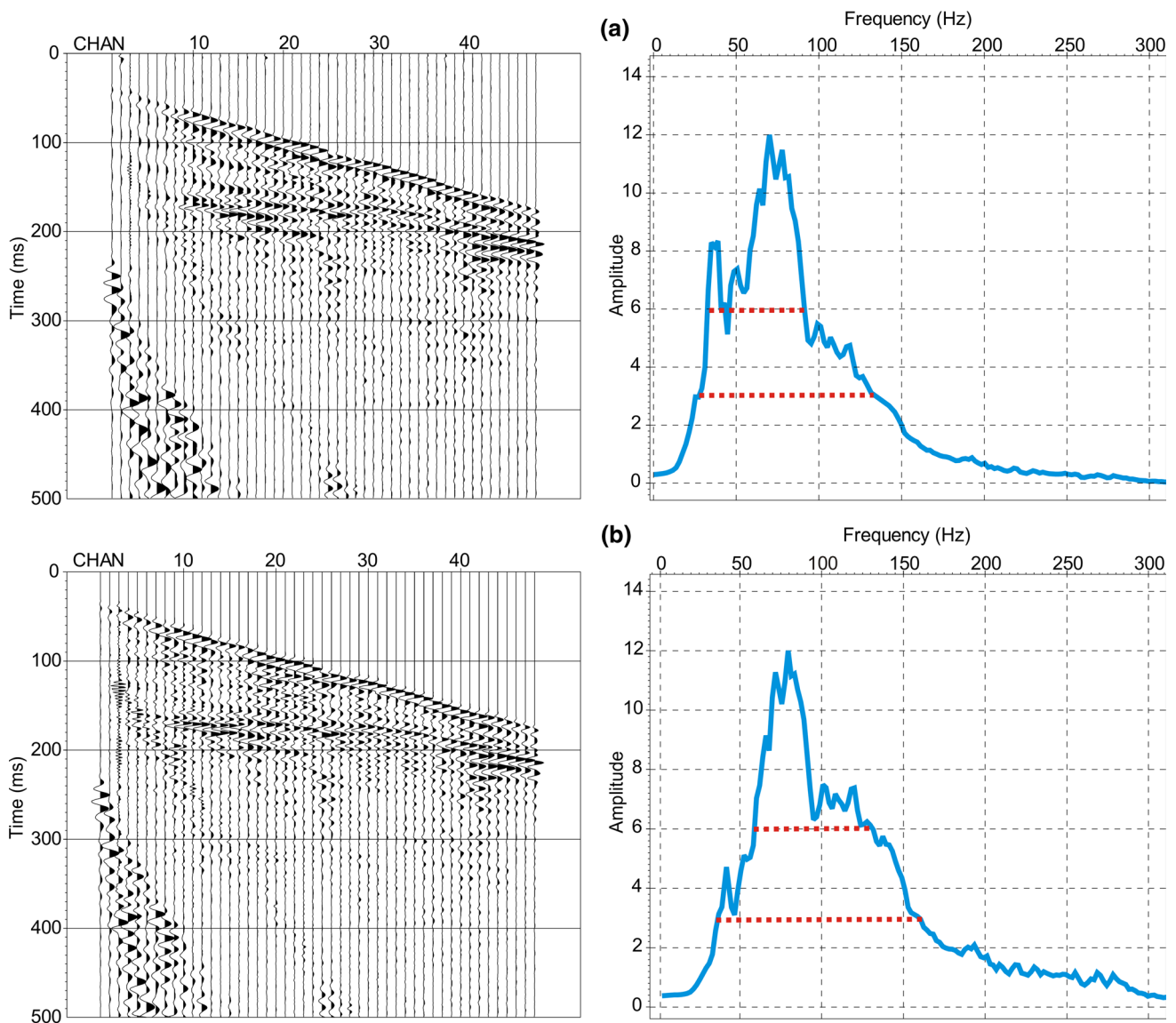


**Fig. 3** The comparison of normalized test field records utilizing **a** 14-Hz and **b** 100-Hz geophones and corresponding mean spectra. With concern to the spectra,  $-6$  and  $-12$  dB bandwidths are marked

(1986a), 100-Hz geophones perform better in the 75–500 Hz bandwidth (Fig. 3b) and attenuate unwanted low-frequency signals. The operating characteristics of high-frequency geophones are better than those of low-frequency geophones, when recording in the same ground motion.

With the use of 100-Hz geophones, much high-frequency noise can be registered, especially when the conditions for a shot are poor (wet soil, uneven surface, etc.). To overcome this problem, vertical stacking should be performed. Five or more stacks are sufficient to obtain noise-free field recording (Fig. 3).

To obtain high-resolution data, the authors decided to use geophones of higher frequency characteristics.

by red lines ( $-6$  dB corresponds to the amplitude value of 6 at maximum spectrum equaling 12)

### Acquisition parameters

For high-resolution imaging, it is of paramount importance to design the acquisition parameter to a specific geological target. In our case, the scope of the seismic survey was the recognition of the Tertiary deposits of depths reaching app. 200 m. Acquisition parameters are presented in Table 1. The source used was ESS-500 Turbo. The active spread was of 48 channels with vertical 100-Hz geophones and 2-m channel spacing. Before planting the geophones, we additionally removed grass to uniform the conditions along the whole line—such a method improves the S/N ratio and limits the changes of wavelet signature. The shot interval was 4 m.

**Table 1** Seismic acquisition parameters

Source type	ESS-500 Turbo (accelerated weight drop)
Recording system	Geometrics Geode
Receiver	Single vertical 100-Hz geophone
Geometry	Variable end-on roll-along spread
Vertical stacks	3 times average, max up to 10
Receiver interval	2 m
Shot interval	4 m
CDP interval	1 m
Live channels	48
Absolute offset range	0–134 m
Nominal fold	12
Sampling	1 ms
Record length	512 ms

Usually, the vertical stack (up to 3 times) was sufficient to obtain satisfactory results. In places where the ground was loose, more than three stacks were performed.

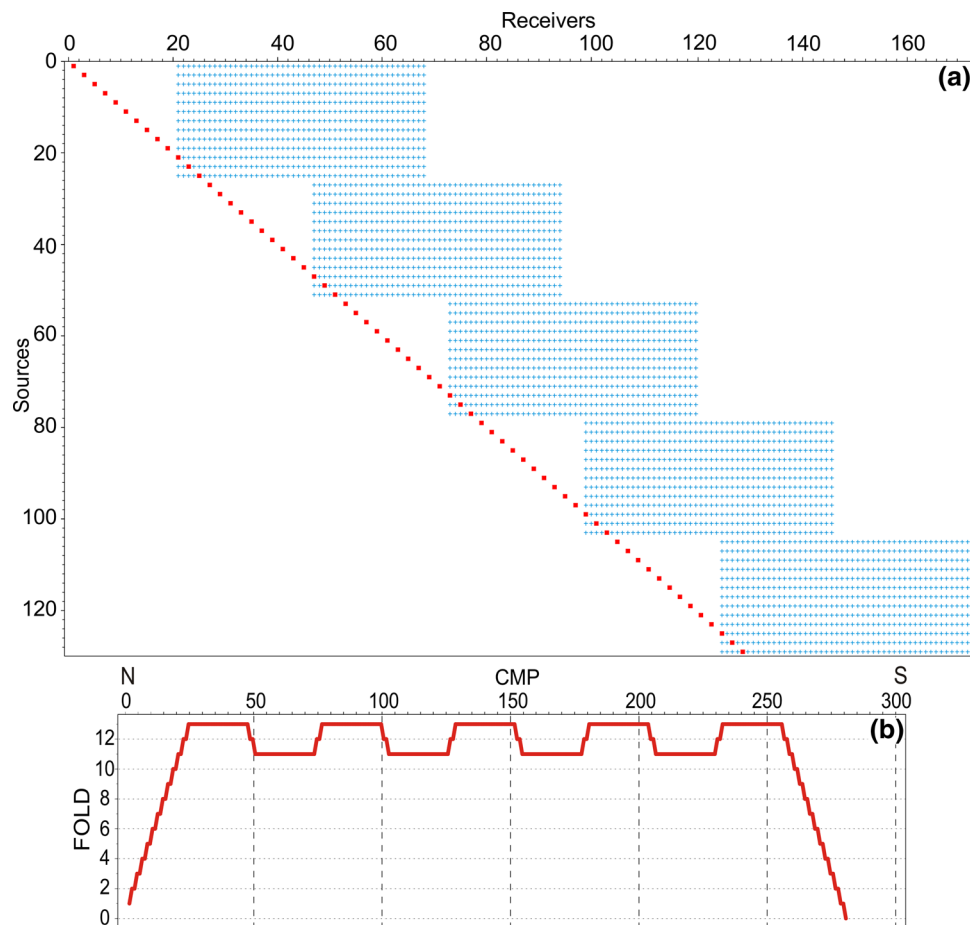
An end-on spread with variable offset was designed. The initial absolute offset range was between 40 and 134 m. Acquisition geometry was designed to obtain maximum

offset, greater than 120 m, which is necessary to obtain correct NMO value ( $NMO \approx 1.5T_{dom}$ , where  $T_{dom}$  is a dominant period) related to reflectors in depth range of 100–200 m. At the same time, near offsets are necessary for imaging of shallow reflectors. After setting the shot point to the fifth channel (offset range between  $-8$  to  $+86$ ), the spread was changed. The acquisition scheme (stacking chart) is presented in Fig. 4a, and the fold distribution (11–13) along the profile is shown in Fig. 4b.

The acquisition designed enabled us to obtain results of good quality with a satisfactory signal-to-noise ratio. The optimal acquisition parameters and proper offset distance, causes the coherent noise—surface wave and air-wave to appear at times greater than the target time (see Fig. 3).

In such a case, amplitudes of these waves (i.e. surface and air waves) do not disturb the response from the geological target and do not have to be cut out at the processing step. Often the procedures that filter out coherent noises influence the amplitude relation that is unfavorable (Yilmaz 1987; Steeples and Miller 1998). The choice to use the end-on spread, instead of the split-spread, enables longer offsets, which is essential for reservoir properties, reasoning basing

**Fig. 4** Field acquisition scheme of the experimental seismic profile. **a** Stacking chart (blue crosses—receivers, red squares—shots); **b** fold distribution of experimental seismic profile. The total number of shots was 65 with 48 receivers active per cable which gives nominal fold 12



on AVO (Amplitude vs. Offset) analysis (Chopra and Castagna 2014; Dec and Cichostępski 2017a).

In the case of the profile, the shot offset was variable, and not all field records hold the criterion for coherent noise (surface and air waves) to be below the time to the target. Nevertheless, 12 traces within one CDP (common depth point) are sufficient to easily reduce the level of unwanted linear events in the stacking process. Residuals from these noises may be effectively filtered on the stacked seismic section.

## Data processing

Data processing aimed at relative amplitude preservation (RAP) is much more rigorous than processing path for structural interpretation purposes. The RAP processing should compensate the energy loss, reduction in coherent and non-coherent noises, reduction in the influence of low velocity layer and complete reduction in all artefacts on seismic traces caused by the processing steps themselves.

It is important not to introduce any procedures that can change the shape and amplitudes of the wavelet. The resulting volume (CDP gathers and stacks) should preserve the true reflectivity of the subsurface (true amplitude processing). It is hardly possible not to affect the reflectivity, and it is a commonly accepted practice to maintain only relative amplitudes; hence, the processing sequence is relative amplitude processing (RAP processing). RAP processing sequence should apply to all procedures to satisfy Shuey's equations (Shuey 1985; Cambois 2001; Aki and Richards 2002; Chopra and Castagna 2014). Usually, a standard path of processing is applied (Resnick 1993; Yilmaz 2001), but some procedures must be adjusted, especially if the target lies within shallow depths (Steeple and Miller 1998). In RAP processing, the only amplitude recovery procedures that can be applied are surface-consistent scaling and spherical divergence correction. AGC, time-variant scaling, etc., do not apply in RAP processing; furthermore, 2D filters, e.g. median, FK, etc., should not be applied, since it can disturb relative amplitudes (see "Appendix").

The applied processing sequence is presented in Table 2. The aim of data processing was to obtain a satisfactory signal-to-noise ratio, high resolution with minimal influence on the seismic wavelet in order to keep RAP criterion. Seismic processing was realized in Vista 2D/3D Seismic Data Processing (Schlumberger).

The initial pre-processing procedures include data format change, geometry adjustments, high-line rejection of 50 Hz (due to electric lines near the study area), spherical divergence correction, refraction statics and first break muting.

**Table 2** Seismic processing sequence

Reformat
Geometry and trace edit
High-line frequency rejection (50 Hz)
Geometric divergence correction (offset dependent)
Refraction statics
First break muting
Surface-consistent amplitude scaling (source and receiver)
Surface-consistent spike deconvolution (source and receiver)
Bandpass filtering (40/60–200/250 Hz)
Datum (floating)
Velocity analysis
NMO
Automatic residual statics
NMO
Trim statics
Bandpass filtering (40/60–200/250 Hz)
Stack
Phase rotation
Signal enchantment with the preserved signal (4D-DEC)
Time-depth conversion

The gradual loss of amplitude, resulting from geometrical spreading, is a significant effect which needs compensation. For RAP processing purposes, appropriate amplitude compensation is required. The correction is achieved by approximating the effect of amplitude loss due to waveform divergence. According to Ursin (1990), geometrical spreading manifests itself by amplitude loss with an increasing offset. For far offsets and shallow seismic boundaries, the loss is substantial. Because of this, apart from applying time correction, offset correction was also applied. With offsets of up to 134 m, it is especially valid for imaging layers within depths between 30 and 150 m.

With the use of 100-Hz geophones, low-frequency components become limited, but the amplitudes of the surface wave can still be high in unfavorable circumstances (i.e., soft soil, wet soil, uneven surface). Application of the previously mentioned correction, compensating geometrical spreading, also influences the surface wave which results in its greater amplitudes (Fig. 5a), showing the exemplary field record where the surface wave corresponds to the first spectral peak at 25 Hz. The influence of the surface wave will be reduced by applying a bandpass filter.

Refraction statics were calculated employing the routine approach, from slopes and intercept times of picked first breaks. We have defined a two-layer velocity model; the estimated velocity in the first layer was 600 m/s, and in the second 1750 m/s. After static correction, we carefully removed first breaks by a top mute with the preservation of wide-angle shallow reflections.

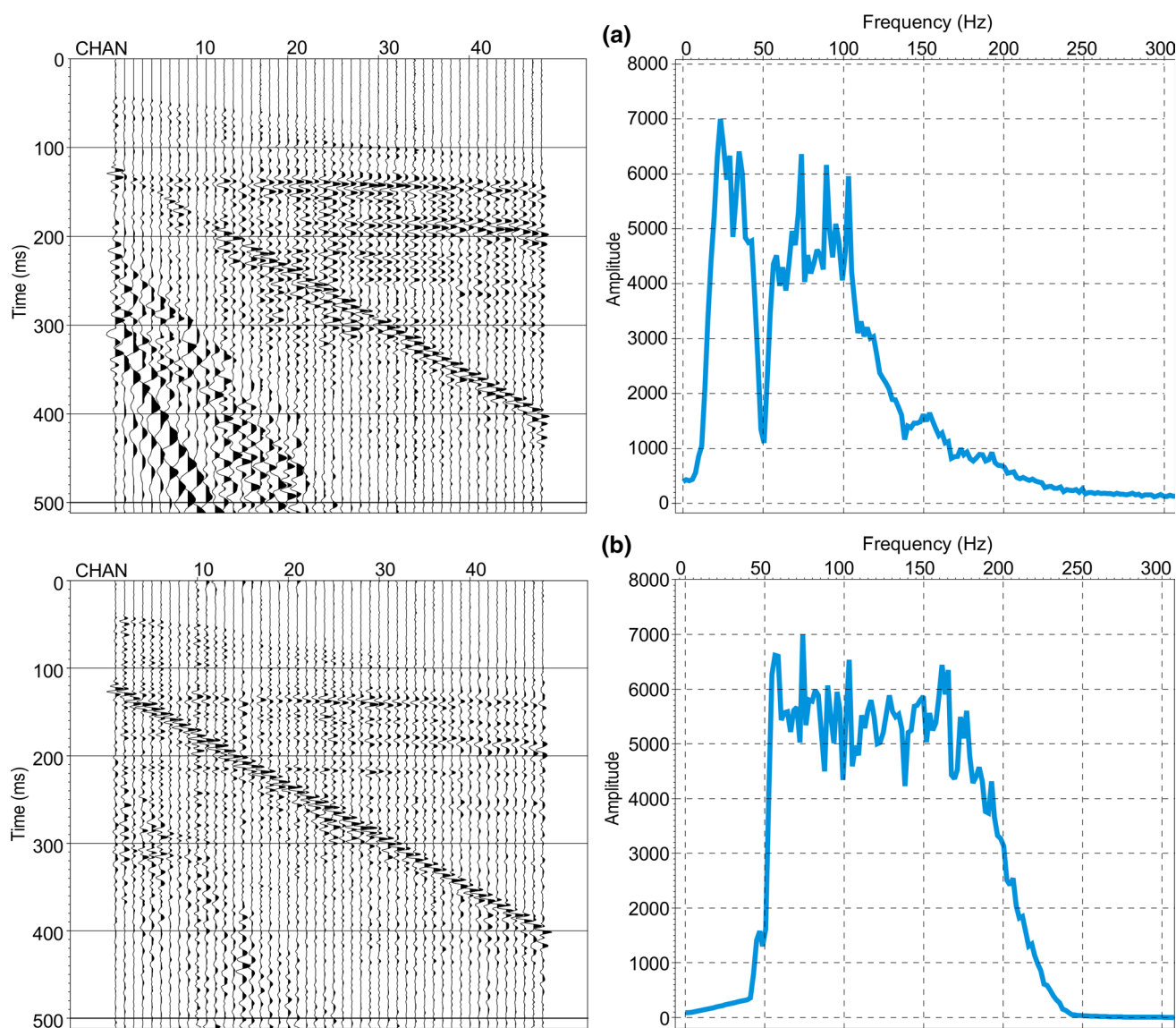


**Fig. 5** Exemplary shot record and its average amplitude spectra after **a** spherical divergence correction and **b** surface-consistent deconvolution and bandpass filtering (40/60–200/250 Hz)

In RAP processing, variability of reflection amplitudes in land seismic should be caused only by changes in petrophysical parameters between layers. However, variability in amplitude, phase and frequency partially depends on changes in source and receiver conditions. For example, unconsolidated material (e.g., sand or mud) at shot or receiver can significantly change the character of amplitude at that particular location compared to an adjacent position that is of a hard ground surface. As a consequence, changing near-surface conditions deteriorate repeatability of the source. Also, differences in receiver coupling can distort the seismic signal. To compensate for these effects, a surface-consistent method is used (Taner and Koehler 1981). The surface-consistent approach means that a single operator is

applied for all traces that have the same surface point in common (e.g., all traces within a single shot or receiver). The operator is solved by Gauss–Seidel iterative process.

To compensate for the effects of variations in source and receiver conditions and the coupling of seismic record amplitudes, we applied surface-consistent amplitude scaling. In this process, the average amplitude of each trace is computed, and the computed trace scalar is assumed to be a multiplication of shot, receiver, offset and CMP. For relative amplitude preservation, only shot and receiver components are used.

Next, for further improving vertical resolution and balancing the amplitude spectra, a surface-consistent spike deconvolution was applied. The length of the operator was



set to 50 ms. The surface-consistent approach in deconvolution compensates for near-surface wavelet distortion. The average wavelet of each trace is assumed to be a convolution of shot, receiver, offset and CMP wavelet. Subsequently, the deconvolution operator is calculated from the amplitude spectra of the chosen components. Similarly to surface-consistent amplitude scaling, for relative amplitude preservation only shot and receiver components were used (Cary and Lorentz 1993). After surface-consistent deconvolution, the 40/60–200/250 Hz bandpass filtering was applied.

In Fig. 5b, the resulting shot after the application of these procedures is presented. The spectrum is flattened within 50–200 Hz, and the dominant frequency is approximately 125 Hz. Spectrum has white character.

After deconvolution process, the seismic data were moved to floating datum, which was set to smoothed ground elevation. The standard procedures of normal move-out corrections (NMO) and velocity analysis were applied. After NMO, we estimated and applied surface-consistent residual statics by Stack Power Maximization algorithm (Ronen and Claerbout 1985). In this case, the surface-consistent approach means that one time correction is computed and applied to all traces within a single shot and a separate correction for all traces that come from a single receiver. Next, the static shifts are added together and applied as a single correction to a trace. The algorithm uses the model correlation technique. It works by creating a cross-correlation between input traces (CMP gather) and model traces (the corresponding summary trace on high S/N ratio stacked seismic section). The model for correlation was obtained by FX deconvolution. Afterward another velocity analysis, NMO corrections, trim statics and bandpass filtering of 40/60–200/250 Hz were applied. Phase rotation enabled the obtaining of zero-phase data. The resulting stacked profile is presented in Fig. 6a. The resulting stack has a moderate signal-to-noise ratio, which is related to low fold parameters, characteristic for shallow seismic. The noise distribution is mostly random; only weak transverse lines can be seen (residual air and surface wave noises) that were not eliminated by the stacking process. In the edges of the profile (where the fold parameter is less than six), and within a time range between 0 and 80 ms (where an effective fold is less than eight), noise is more visible and masks the reflectors. To preserve real amplitudes, the denoising process must be performed with great control and without any changes in the wavelet form. In “Appendix,” we compare and discuss denoising procedures that are commonly used in shallow seismic. As an optimal denoising method for RAP processing, we propose the 4D-DEC procedure (Butler 2012). The 4D-DEC algorithm employs principal component decomposition in the time domain. In opposition to the frequency domain (which mostly is used for data denoising, for example, FX or FK algorithms), within the time domain the

signal can be easily recognized by its similarity trace by trace within the time window. Because of this prediction, the signal can be nonlinearly, progressively removed. The noise that is left after signal removal can then be moved from the original section with adaptive subtraction.

The 4D-DEC algorithm works by creating wavelet within small overlapping windows in time and space. In each window, a single dip is picked, and the wavelet is created by first break stacking along the chosen dip. Events are then aligned and restocked with correlation statics. With this operation, a high-resolution wavelet is produced. The obtained wavelet is matched in amplitude and time to each trace. The design window time length that we applied was 200 ms, maximum dip 8 ms/trace, filter length consisted of 13 traces and maximum static 5 ms (see “Appendix”). The algorithm preserves fine details of statics and the signal amplitude, while the trace wavelet within the window is constant. In result, 4D-DEC creates a noise model. The volume of noise computed in this way (Fig. 6b) was adaptively subtracted from the input data (Fig. 6a) without damaging the signal. The resulting stack volume is free from noise (Fig. 6c).

## Results and discussion

The surface seismic source ESS-500 generates a wavelet of very high resolving power. The length of the wavelet is usually between 18 and 22 ms, depending on the specific conditions in the field. After the deconvolution process, the wavelet is much shorter and compressed which gives a broad and flat spectrum.

Figure 7 shows the extracted mean wavelet and its spectrum. The wavelet signature is very short and is a minimal-phase wavelet, similar to the Ricker wavelet. Its initial rotation is 35°; length equals 12 ms with 8 ms period (dominant frequency of about 125 Hz).

The processing sequence was designed to maintain a broad frequency spectrum. High frequencies were reconstructed in the deconvolution process, and no invasive methods of signal enchantment were applied, e.g., spectral whitening or bandwidth extension as these procedures disturb relative amplitudes. The average spectrum for the final result is presented in Fig. 8b. The spectrum has a flat character within a range between 50 and 200 Hz. Estimated signal-to-noise ratio along the profile generally ranges from 15 to 30, which we consider as satisfactory. Preservation of relative amplitudes allows for the correlation of changes in amplitudes along seismic horizons with changes of petrophysical parameters. With such a result, one can proceed with qualitative analysis and interpretation.

The final stack with interval velocities displayed in the background is shown in Fig. 8a. For display purposes, a mean amplitude scaling was applied for all the traces with

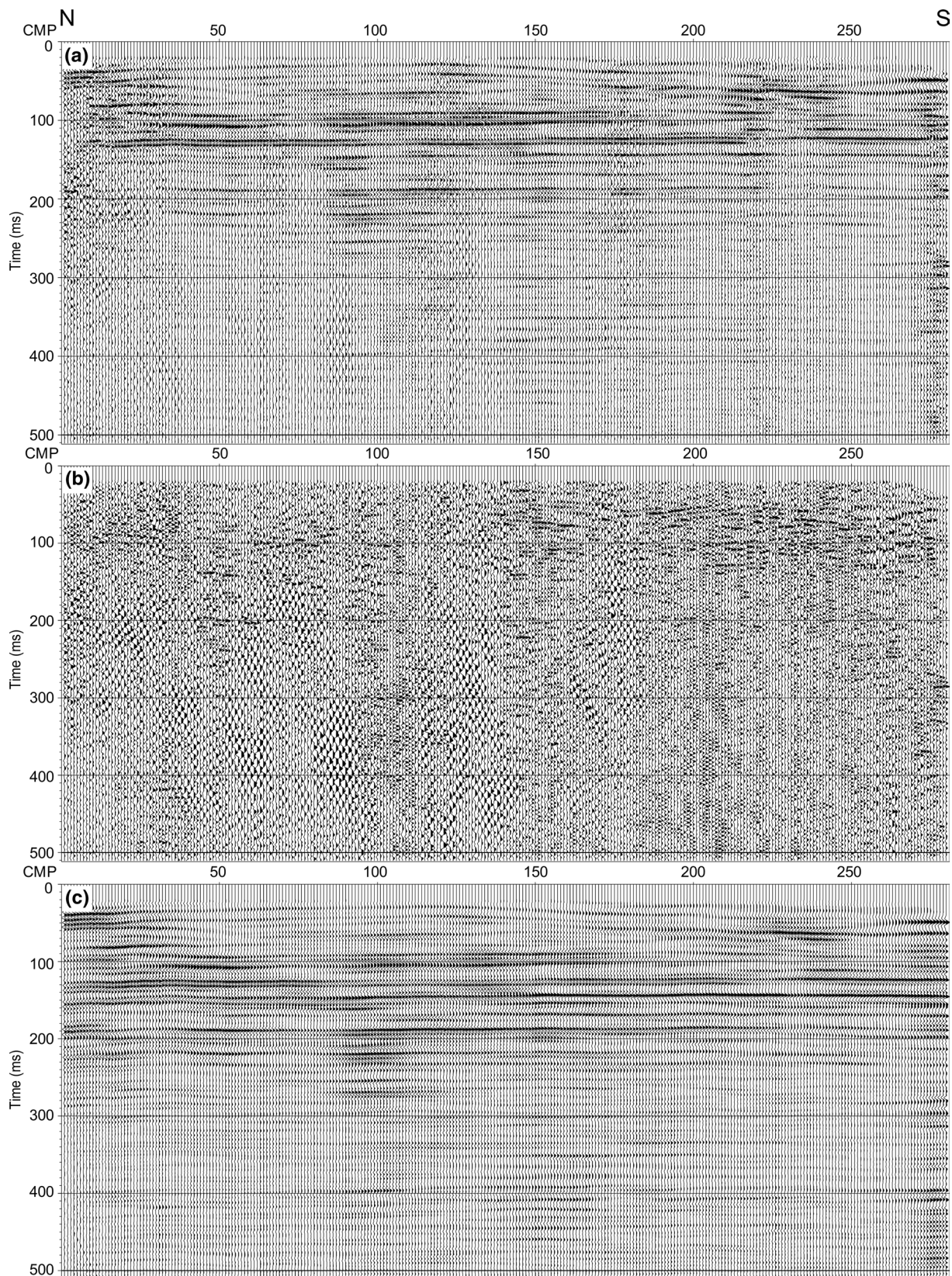
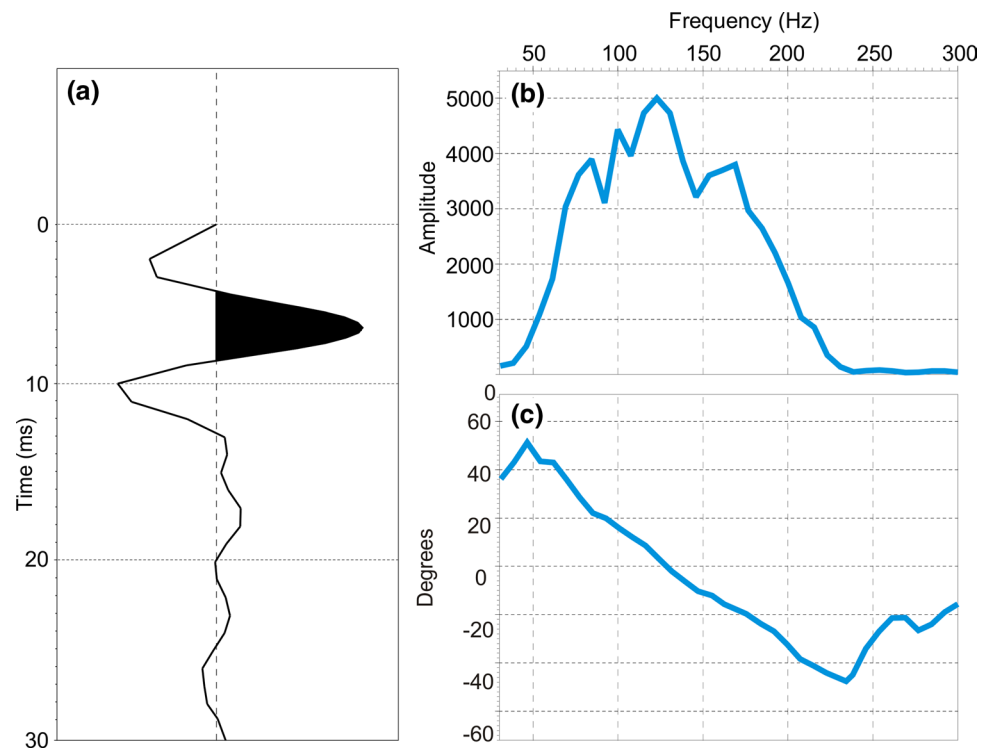


**Fig. 6** Results of noise suppression by using 4D-DEC algorithm: **a** stack, **b** noise model, **c** stack after adaptive subtraction of noise

**Fig. 7** **a** Extracted average wavelet with **b** amplitude spectrum and **c** phase spectrum



a single scalar. Therefore, relative amplitudes are preserved across the section. The middle frequency for the final stack, similarly to the extracted wavelet, is about 125 Hz, which in our case gives a high resolution. For the Tertiary sediments (20–380 ms), the interval velocities around 1400–2000 m/s (Fig. 8a) for the dominant frequency of 125 Hz correspond to the wavelength ( $\lambda$ ) of 11–16 m. With the resolution criteria given by Widess (1973), the limit of resolution for thin layers is equal to  $\lambda/4$  for 2D seismic data. In the extreme case, i.e., for thin coal beds that have very low velocities (c.a. 1250 m/s) and have opposite reflection coefficients in their tops and beds, the minimal thickness that can be resolved is 2.5 m.

Figure 9 shows an analyzed seismic profile after time-depth conversion. For the conversion, a smoothed version of estimated velocities was used (velocities are shown in the background of Fig. 8a). In CMP # 50, there is a simplified stratigraphic chart based on geological information that comes from a nearby wellbore S-419 (location shown in Fig. 1). The seismic horizons within the Pliocene sediments (20–80 m) are sagged, which is associated with the post-glacial structural deformations of these deposits. The first strong seismic reflection (negative polarization) at a depth of 90 m represents the top of the Henryk brown coal bed that has a thickness of about 10 m. The Henryk coal bed closes the Miocene sediments.

Beneath, in the Miocene interval two coal beds are interpreted: first the Łużycki coal bed (thickness of about 10 m) and second in depth the Ścinawski coal bed of a thickness

of 5 m (which is very close to the resolution limit of 2.5 m). In Fig. 9, we also present an enlarged image of the Łużycki and Ścinawski coal beds. The thickness of the Łużycki bed is approximately equal in wavelength, which makes the resulting resolution high, whereas the thickness of the Ścinawski bed is approximately equal to half of the wavelength.

Other seismic horizons visible at section are associated with layers of argil and gravels. At a depth of about 320 m, there is a weak reflection corresponding to the top of the Głogowski coal bed (the top of a thin Eocene complex). Between depths of 340 and 360 m lies the seismic horizon which is linked to the top of the Tertiary deposits.

The seismic image presented in Fig. 9 shows how rapid the energy loss is with increasing depth, when strong seismic boundaries (coal beds) are present. Excepting structural imaging, as a result of RAP processing, we can also observe horizontal variability of a real wavelet's amplitudes along horizons. It is most important for coal prospecting, where these changes can be correlated with facial changes within brown coal seams.

## Conclusions

The test acquisition enabled us to verify that ESS-500 seismic generator is a suitable source for shallow seismic imaging. For Fore-Sudetic monocline's Tertiary sediments, the ESS-500 enables high-resolution data to be

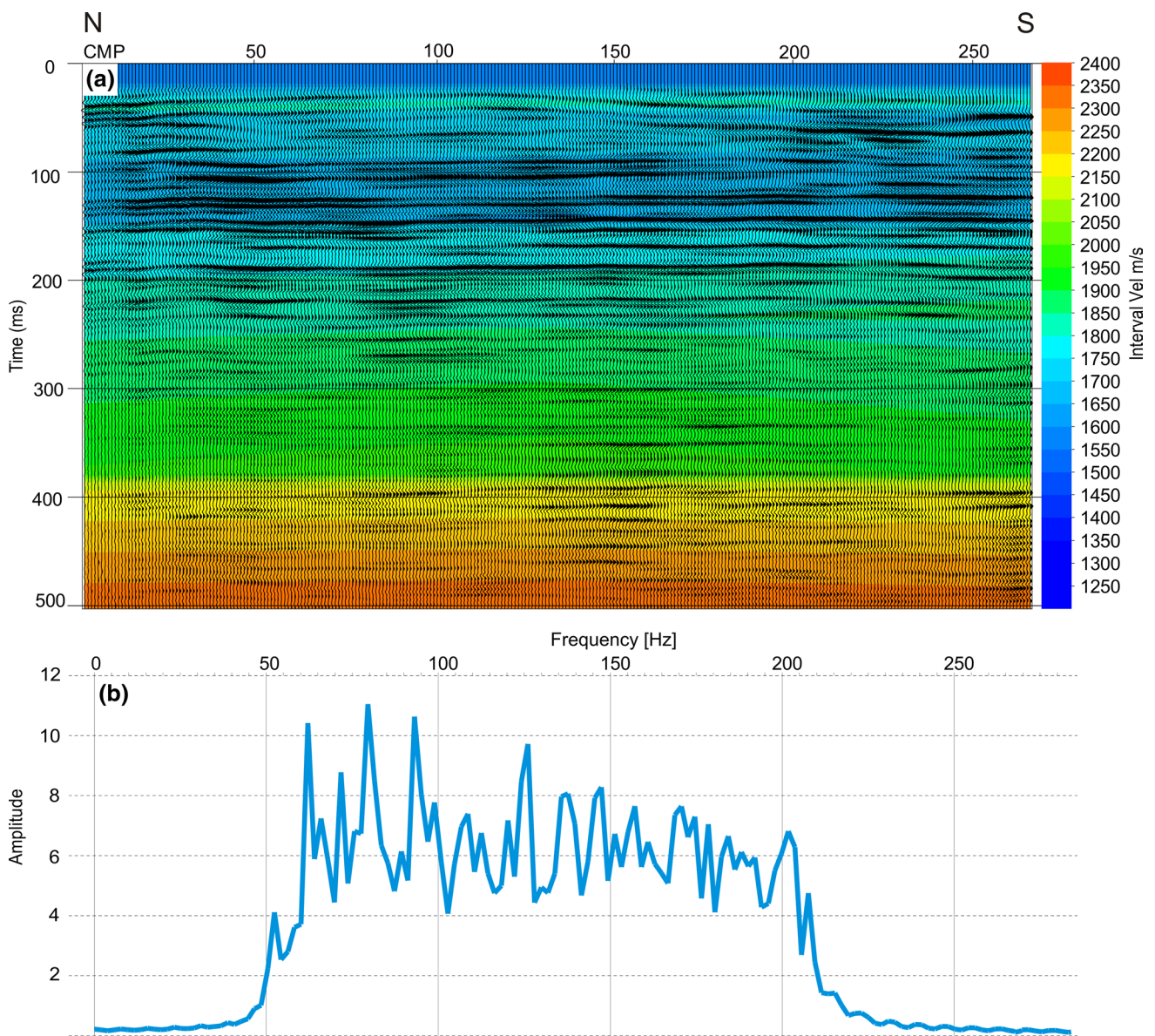


**Fig. 8** **a** Final stack with interval velocity in the background and **b** its average spectrum

obtained. The generated wavelet can be effectively compressed in the deconvolution process, the key step to maintaining high frequencies for the given dataset. The resulting wavelet is very short (40/60–200/250 Hz bandwidth, 8 ms period, 12 ms length). Well-designed seismic acquisition can significantly limit the distortion of the seismic signal at the processing step since coherent noises do not interfere with the geological target.

For the interval velocities of about 2000 m/s and with the middle frequency of 125 Hz, the dominant wavelength is 16 m. In such a case, the limit of resolution reaches at

least 4 m. For brown coal beds of much lower velocities ( $V_p = 1250$  m/s), the limit of resolution decreases to about 2.5 m—this result is exceptionally good for shallow seismic imaging.

A comparison of different denoising methods indicated that the 4D-DEC procedure is the most optimal for maintaining the criteria of relative amplitude preservation.

RAP-processed high-resolution, shallow seismic data may be the appropriate input for further precise recognition of lithofacial changes, and evaluation of petrophysical and geomechanical parameters at the near-surface zone.

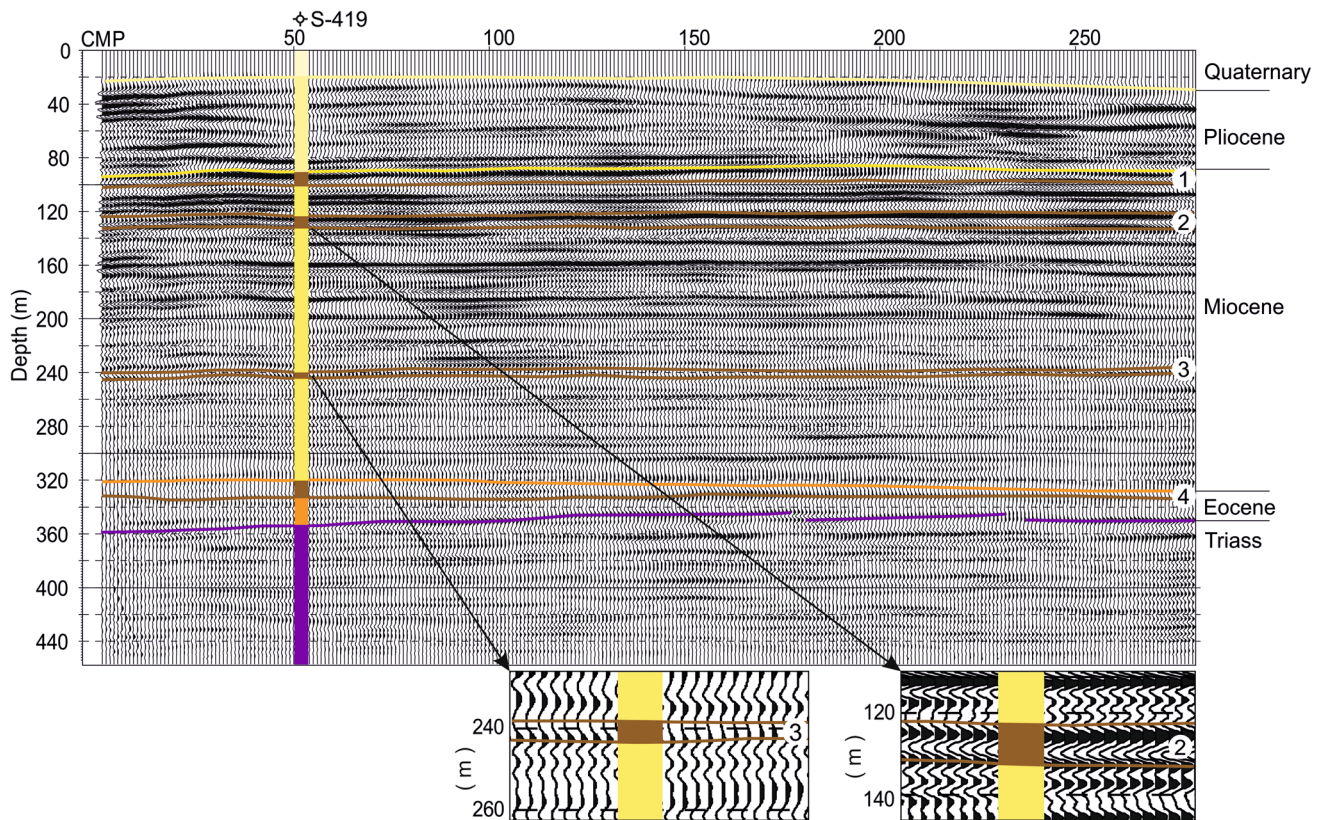


**Fig. 9** Analyzed experimental seismic profile from Fig. 8a after time-depth conversion. 1, 2, 3, 4—brown coal seams: Henryk, Łużycki, Sciniawski, Głogowski. The zoomed parts show Łużycki (10 m) and Sciniawski (5 m thickness) coal seams

**Acknowledgements** The research was supported by the Polish Academy of Sciences via European Plate Observing System (EPOS) project and AGH-UST University of Science and Technology in Krakow, Poland grant no. 11.11.140.645. Vista 2D/3D Seismic Data Processing was provided by the Schlumberger through University Software Grant Program. We would like to thank the editor M. Malinowski and two anonymous reviewers for providing valuable and insightful feedback on the manuscript.

### Compliance with ethical standards

**Conflict of interest** On behalf of all authors, the corresponding author states that there is no conflict of interest.

**Open Access** This article is distributed under the terms of the Creative Commons Attribution 4.0 International License (<http://creativecommons.org/licenses/by/4.0/>), which permits unrestricted use, distribution, and reproduction in any medium, provided you give appropriate credit to the original author(s) and the source, provide a link to the Creative Commons license, and indicate if changes were made.

### Appendix

In some of the chosen field records, the air wave is visible (Fig. 10a). Moreover, the residues of the surface wave which were not entirely reduced in the deconvolution process are also present.

Below, we show procedures that are commonly applied for noise removal in shallow seismic. We evaluate each of them and then decide which are optimal for relative amplitude processing that we applied in Data processing section. All procedures were tested on the same record.

The procedure 4D-DEC that we choose to be optimal can also be applied to the pre-stack data. The application of 4D-DEC procedure enabled the definition of the noise set (Fig. 10b) which was adaptively subtracted from data to create a noise-free record (Fig. 10c). The effectiveness of the 4D-DEC procedure is very good, and its application enables the removal of surface and acoustic waves. Nevertheless, the procedure applied to records distorts the output.

Alternative denoising procedures can be via FK filtering, median filter and surgical muting. Figure 11 shows the application of a FK filter. The rejection zone present in Fig. 11b

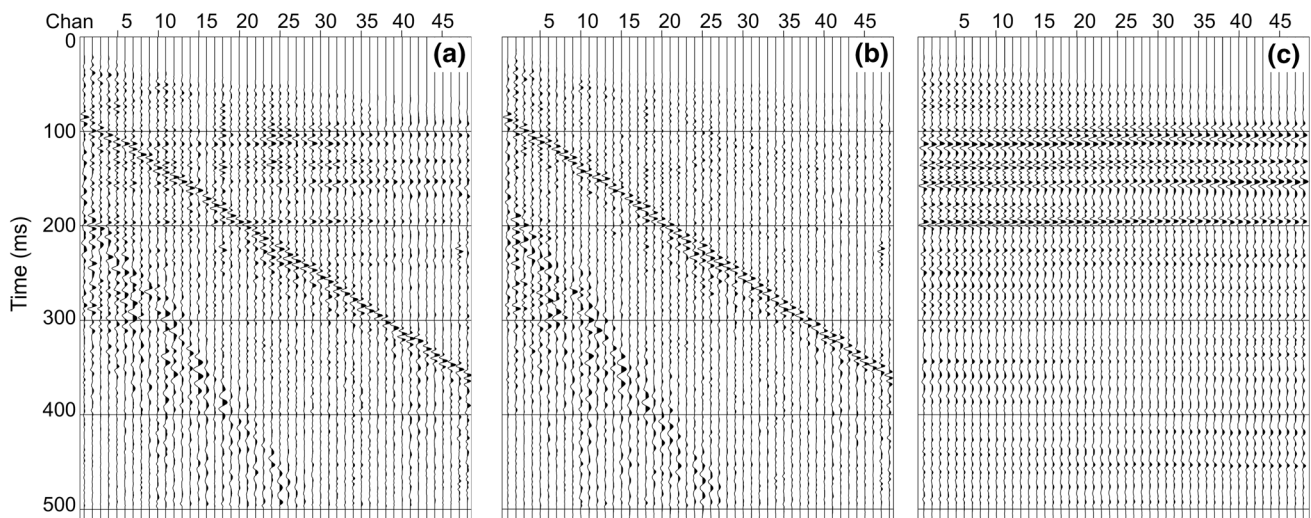


**Fig. 10** Result of applying 4D-DEC. **a** Exemplary record after NMO, **b** extracted noise model, **c** record after adaptive subtraction of noise

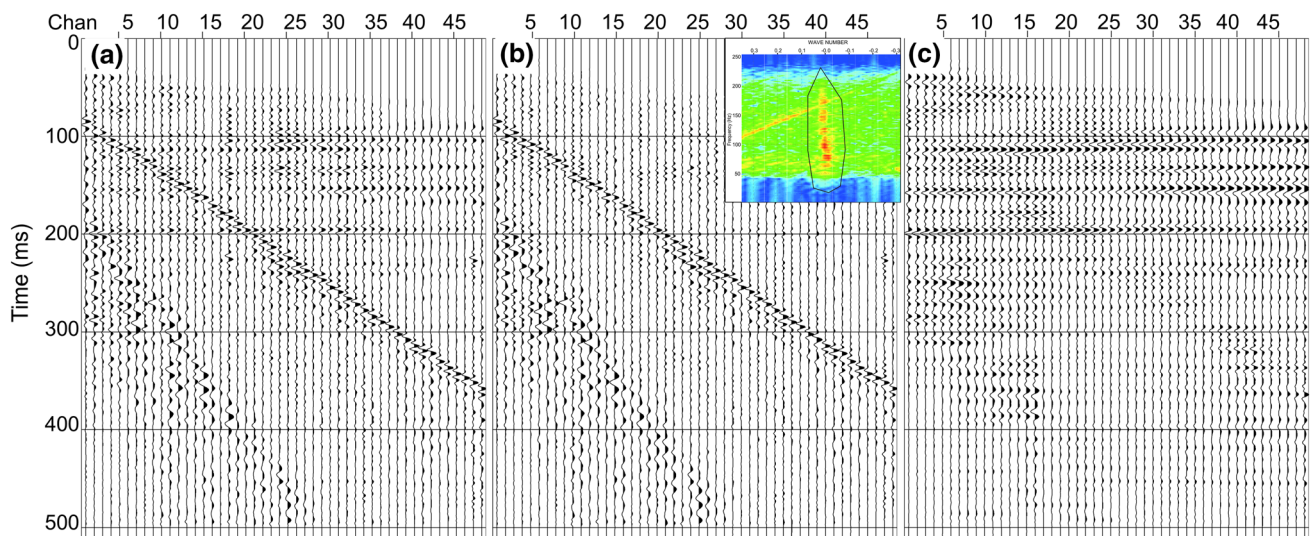


**Fig. 11** Result of applying FK. **a** Exemplary record after NMO, **b** extracted noise model and designed the FK reject filter, **c** record after adaptive subtraction of noise

was used in the FK domain to create a noise model. Next, the extracted noise was adaptively subtracted from the input data. As is shown in Fig. 11c, surface and air waves were not entirely reduced. Corresponding times for these waves manifest themselves by gained amplitudes which will result in non-relative amplitude values after stacking procedure.

In Fig. 12, application of a median filter is shown. We used a 7 traces window. The obtained result (Fig. 12c) and the noise model (Fig. 12b) are similar to the result of FK filtering (Fig. 11b, c). The residue of surface and air waves are still visible. Moreover, application of the median filtering

approach causes high-frequency artifacts. These artifacts have to be filtered out in the additional step.

Figures 13 and 14 present stacked sections after differing processing paths, comparing chosen sequence processing (4D-DEC on the stacked section). The section after median filtering (Fig. 13a), 4D-DEC (Fig. 13b), FK filter (Fig. 14a) and surgical muting (Fig. 14b) which were applied to shot records shows/reveals distortion of amplitude relation, this phenomenon is clearly visible for the horizon that occurs at 150 ms. Also, section after surgical muting (Fig. 14b) is characterized by a lower signal-to-noise ratio as a result of the removal of part of the seismic record (a designed

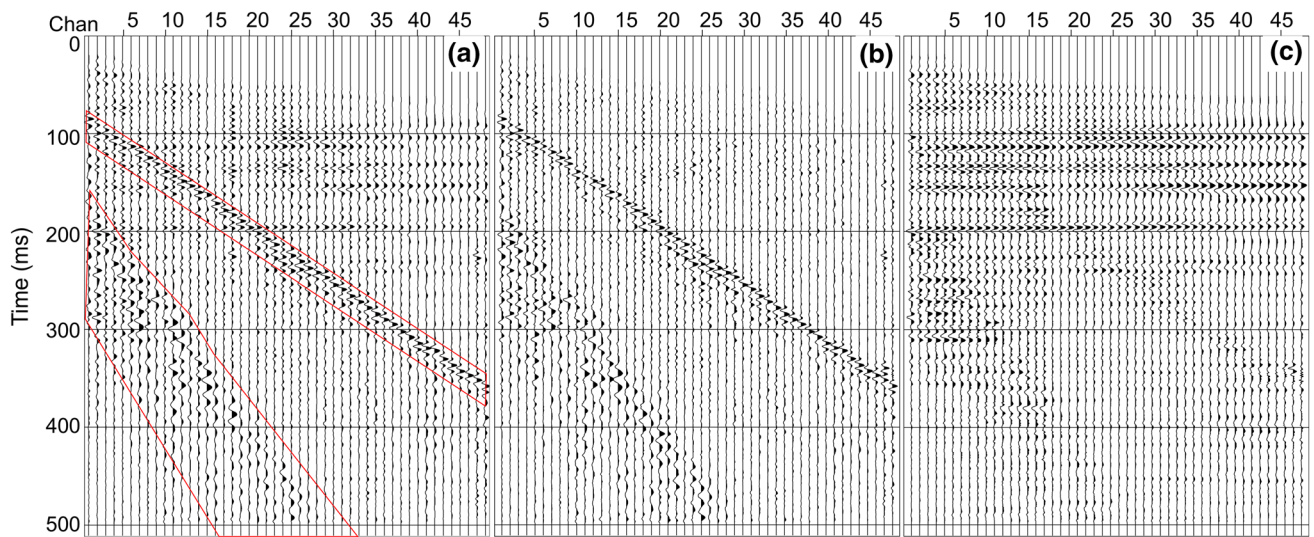


**Fig. 12** Result of applying the median filter. **a** Exemplary record after NMO, **b** extracted noise model, **c** record after the median filter. Red polygons—designed surgical muting; results of surgical muting are presented in Fig. 14b

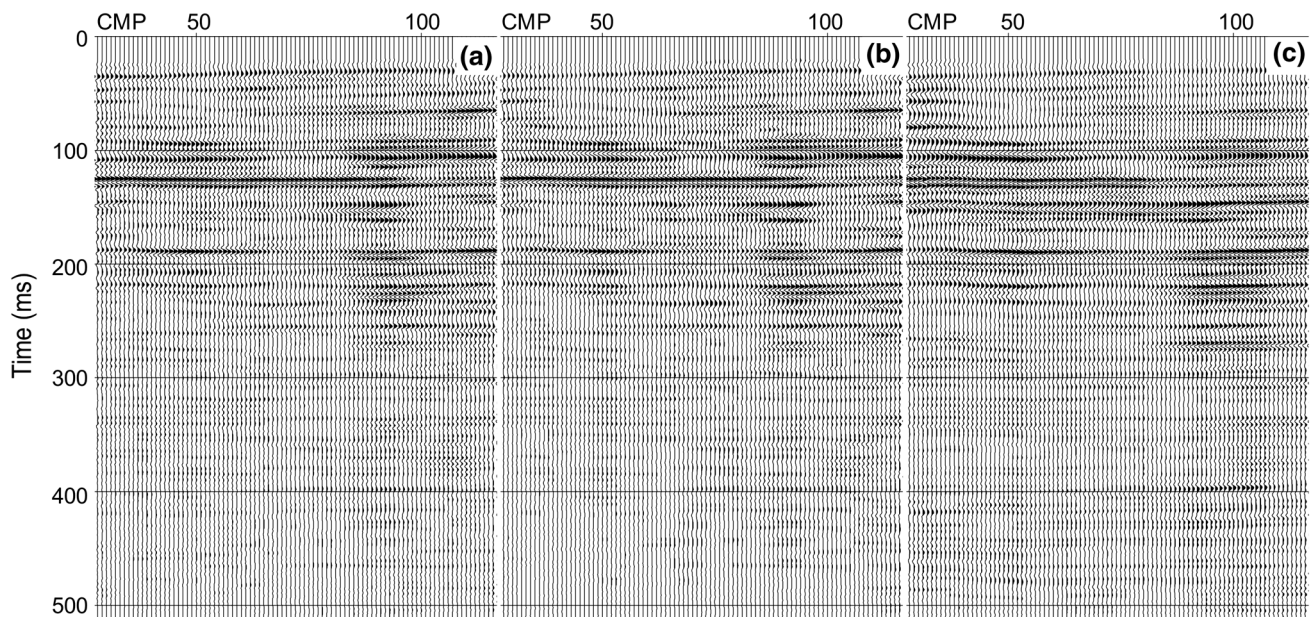


**Fig. 13** Part of time section—comparison of different filtering results. **a** Section after median filter applied to shot records, **b** section after 4D-DEC applied to shot records, **c** section after 4D-DEC applied to the final stack

surgical mute is presented in Fig. 12a as a red polygon). After 4D-DEC is performed on stacked section (Figs. 12c, 13c), the amplitude relation is preserved, and continuity of horizons is improved. Furthermore, after this procedure, the reflection below 300 ms is more visible.

The 4D-DEC process requires careful parameterization. This procedure was described in Data processing section.

We have tested different parameters and their influence on the final result. As the test shows, the most important parameter is the trace window. Figure 15 shows the application of 4D-DEC with different trace windows. The latter parameters were set to: time window—200 ms, maximum dip—8 ms/trace and maximum static—5 ms. The best result was obtained with 13 trace windows (Fig. 15b). A window

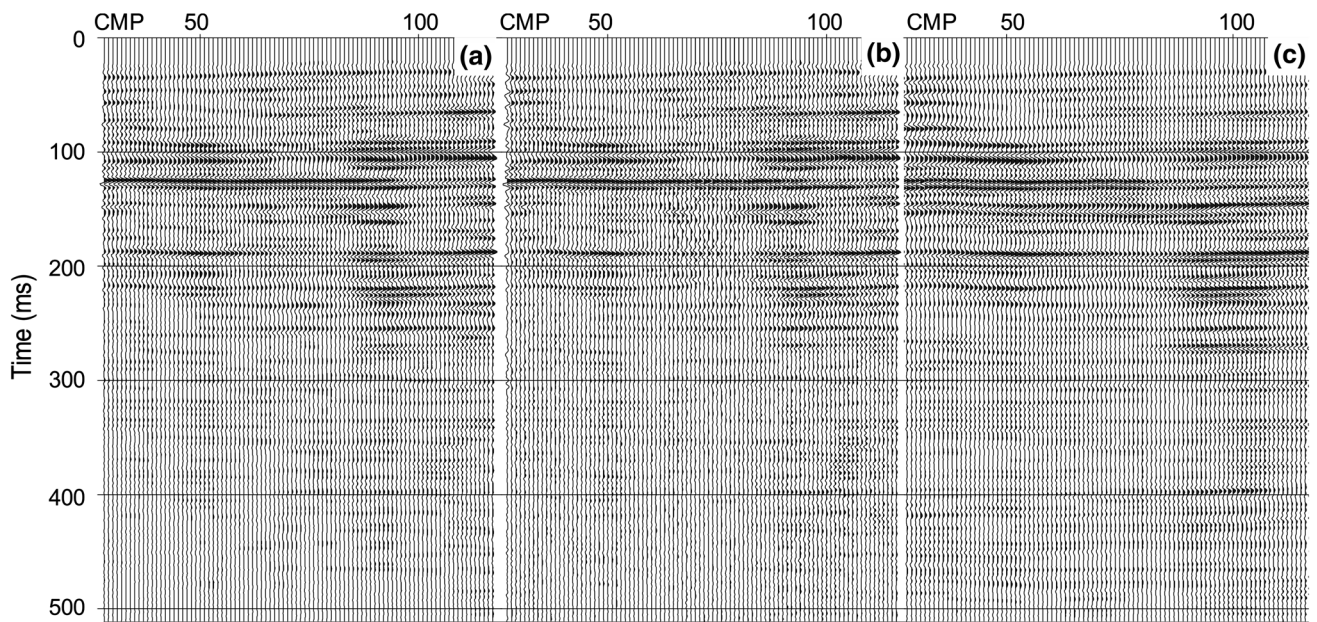


**Fig. 14** Part of time section—comparison of different filtering results. **a** Section after FK filter applied to shot records, **b** section after surgical muting applied to shot records, **c** section after 4D-DEC applied to the final stack

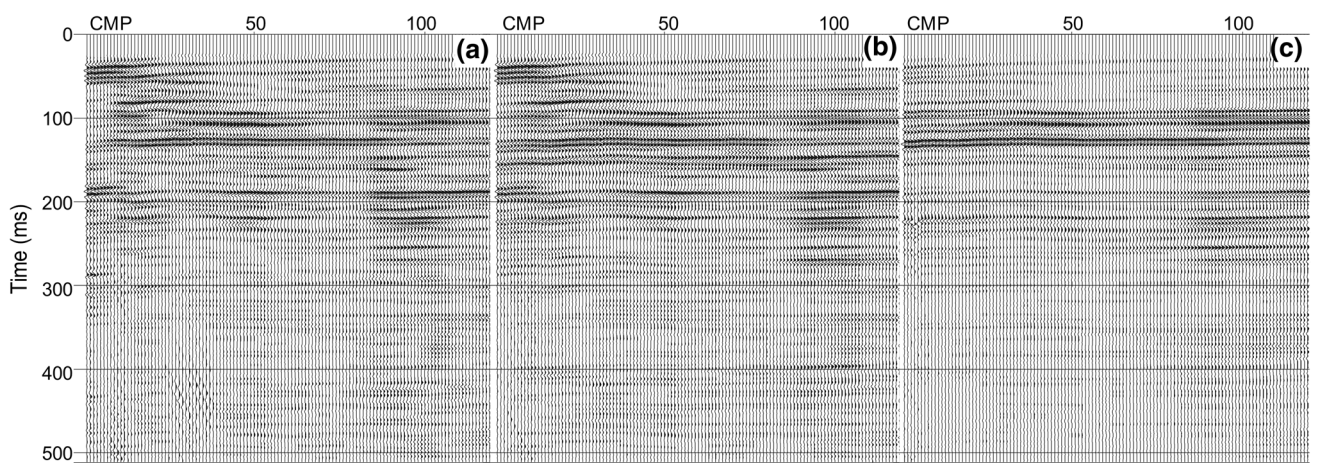


**Fig. 15** Part of time section—comparison of 4D-DEC results for different trace windows parameter. **a** 7 Traces window, **b** 13 traces window, **c** 25 traces window



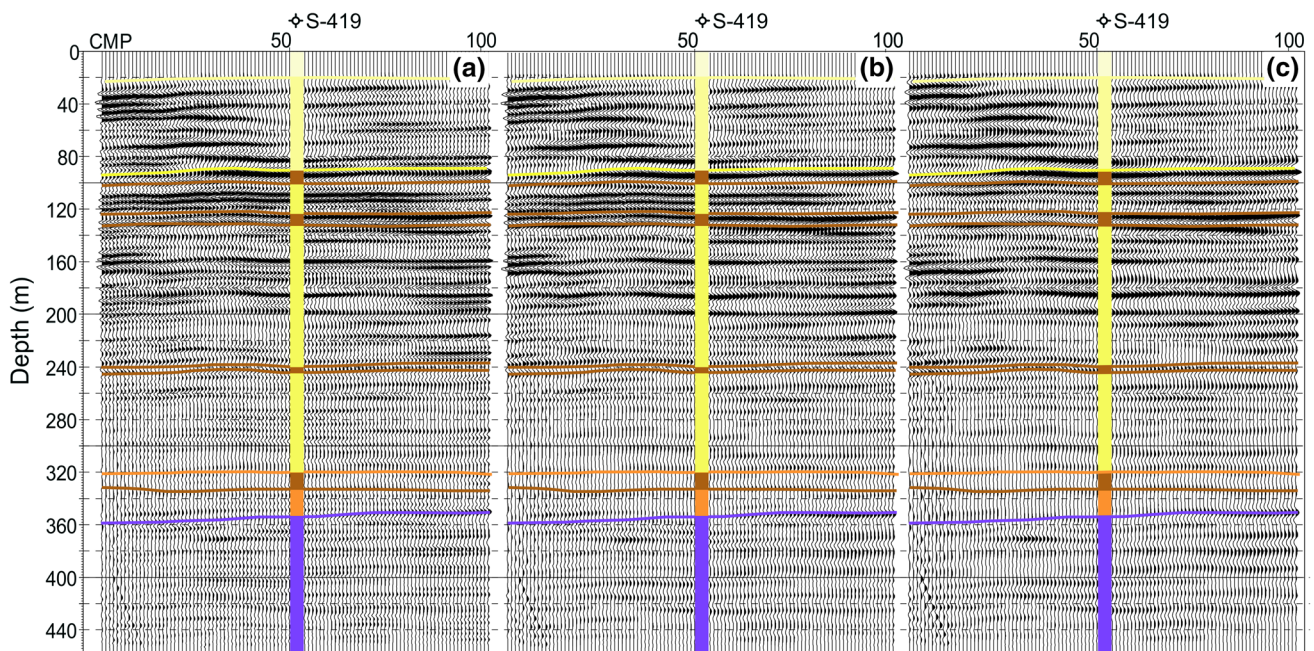


**Fig. 16** Part of depth section near well S-419—comparison of different bandwidth. **a** 40/60–200/250 Hz, **b** 40/60–150/180 Hz, **c** 40/60–120/150 Hz. For horizon description, see Fig. 9

composed of 7 traces (Fig. 15a) does not remove noise completely, and the longest window (25 traces, Fig. 15c) averaged the data and lowered the amplitude values along horizons. As a result, the authors believe that application of 4D-DEC on stacked section rather than on shot records is less invasive and more accurate. For quantitative interpretation of seismic data (AVO, pre-stack inversion), denoising must be performed on CMP collections before stacking with minimizing the smearing effect.

In some cases, the resolution that is too high can deteriorate the image. In our case, we obtain a dominant frequency of 125 Hz and an effective bandwidth of 50–220 Hz. We verified whether the seismic image is appropriate for this bandwidth. To do this, we compared the depth sections obtained for different bandwidths. Figure 16a shows results for the high-cut filter: 200/250 Hz; Fig. 16b for 150/180 Hz and Fig. 16c for 120/150 Hz. As the test results prove, the more narrow frequency range, the more smearing and decrease in resolution are present. Wide bandwidth, i.e., 40/60–200/250 Hz, does not deviate seismic imaging for the interpreted seismic horizons and manifests itself by high resolution.

## References

- Aki K, Richards PG (2002) Quantitative seismology. W.H. Freeman and Company, New York
- Atanackov J, Gosar A (2013) Field comparison of seismic sources for high resolution shallow seismic reflection profiling on the Ljubljana moor (central Slovenia). *Acta Geodyn et Geomater* 10(1):19–40
- Baumgart-Kotarba M, Dec J, Ślusarczyk R (2001) Quaternary tectonic grabens of Wróblówka and Piniązkowice and their relation to Neogene strata of the Orava Basin and Pliocene sediments of Domański Wierch series in Podhale, Polish West Carpathians. *Studia Geomorpho Carpatho-Balcanica* XXXV:101–119
- Baumgart-Kotarba M, Dec J, Kotarba A, Ślusarczyk R (2008) Glacial trough and sediments infill of the Biała Woda Valley (the High Tatra mountains) using geophysical and geomorphological methods. *Studia Geomorphol Carpatho-Balcanica* XLII:75–108
- Benjumea B, Teixido T (2001) Seismic reflection constraints on the glacial dynamics of Johnsons Glacier. *Antarct J Appl Geophys* 46:31–44
- Berkhout AJ (1985) Seismic resolution: a key to detailed geologic information. *World Oil* 201:47–51
- Butler P (2012) White noise suppression in the time domain. *CSEG Rec* 37(9):39–44
- Cambois G (2001) AVO processing: myths and reality. *CSEG Rec* 26:30–33
- Cary PW, Lorentz GA (1993) Four-component surface-consistent deconvolution. *Geophysics* 58:383–392
- Chopra S, Castagna JP (2014) AVO. Investigations in geophysics. Society of Exploration Geophysics, Tulsa
- Dec J (2012) High-resolution seismic survey for recognition of the Osiek sulphur deposits and determination of dynamic changes resulting from exploitation. Wydawnictwa AGH, Kraków [in Polish with English abstract]
- Dec J, Cichostępski K (2017a) Evaluation of sulphur deposit properties on the basis of geomechanical parameters. *Zeszyty Naukowe Instytutu Gospodarki Surowcami Mineralnymi i Energią PAN* 101:203–216 [in Polish with English abstract]
- Dec J, Cichostępski K (2017b) Estimation of sulphur deposit resources on the basis of seismic data. *Zeszyty Naukowe*

- Instytutu Gospodarki Surowcami Mineralnymi i Energią PAN 101:217–227 [in Polish with English abstract]
- Francesc RG, Hajnal Z, Schmitt D, Zaja A (2007) High resolution seismic reflection imaging of complex stratigraphic features in shallow aquifers. *Memorie Descrittive della Carta Geologica d'Italia LXXXVI*:175–192
- Gisco (2018) Documentation of Gisco vertical geophones. <http://www.giscogeo.com/products-equipment/geophones>. Accessed 31 July 2018
- Kłapciński J, Peryt TM (2007) Budowa geologiczna monokliny przedsudeckiej. Monografia KGHM Polska Miedź SA 69–77
- Kłapciński J, Konstantynowicz E, Salski W, Kenig E, Preidl M, Dubiński K, Drozdowski S (1984) Atlas obszaru miedzionośnego (monoklina przedsudecka). Wydawnictwo Śląsk, Katowice
- Knapp RW, Steeples DW (1986a) High-resolution common-depth-point seismic reflection profiling: instrumentation. *Geophysics* 51(2):276–282
- Knapp RW, Steeples DW (1986b) High-resolution common-depth-point reflection profiling: field acquisition parameter design. *Geophysics* 51(2):283–294
- Kwietniak A, Cichostępski K, Pietsch K (2018) Resolution enhancement with relative amplitude preservation for unconventional targets. *Interpretation* 6(3):SH59–SH71
- Miller RD, Pullan SE, Waldner JS, Haeni FP (1986) Field comparison of shallow seismic sources. *Geophysics* 51(2):2067–2092
- Miller RD, Steeples DW, Brannan M (1989) Mapping a bedrock surface under dry alluvium with shallow seismic reflections. *Geophysics* 27:1528–1534
- Miller RD, Steeples DW, Myers PB (1990) Shallow seismic reflection survey across the Meers fault, Oklahoma. *Bull Geol Soc Am* 102:18–25
- Miller RD, Pullan SE, Steeples DW, Hunter JA (1992) Field comparison of shallow seismic sources near Chino, California. *Geophysics* 57(5):693–709
- Miller RD, Pullan SE, Steeples DW, Hunter JA (1994) Field comparison of shallow P-wave seismic sources near Houston, Texas. *Geophysics* 59(11):1713–1728
- Myers PB, Miller RD, Steeples DW (1987) Shallow seismic reflection profile of the Meers fault, Comanche County, Oklahoma. *Geophys Res Lett* 15:749–752
- Palmer D (1987) High resolution seismic reflection surveys for coal. *Geoexploration* 24:397–408
- Požaryski W (1979) Mapa geologiczna Polski I krajów ościennych 1:1000000. Wyd. Geologiczne, Warszawa
- Resnick JR (1993) Seismic data processing for AVO and AVA analysis. In: Castagna JP, Backus MM (eds) *Offset-dependent reflectivity—theory and practice of AVO analysis*. Society of Exploration Geophysics, Tulsa, pp 175–189
- Ronen J, Claerbout JF (1985) Surface consistent residual statics estimation by stack power maximization. *Geophysics* 50(12):2759–2767
- Sheriff RE (1985) Aspects of seismic resolution. In: Berg OR, Woolvetron DG (eds) *Seismic stratigraphy II: an integrated approach to hydrocarbon exploration*. AAPG Memoir 39
- Sheriff RE (1991) *Encyclopedic dictionary of exploration geophysics*. Society of Exploration Geophysics, Tulsa, p 240
- Sheriff RE (1997) Seismic resolution: a key element. *AAPG Explor Geophys Corner* 18:44–51
- Shuey RT (1985) A simplification of the Zoeppritz equations. *Geophysics* 50(4):609–614
- Singh S (1984) High-frequency shallow reflection mapping in tin mining. *Geophys Prospect* 32:1033–1044
- Steeple DW, Miller RD (1990) Seismic reflection methods applied to engineering, environmental, and groundwater problems. In: Ward S (ed) *Review and tutorial: investigations in geophysics*, vol 5. Society of Exploration Geophysicists, Tulsa, pp 1–30
- Steeple DW, Miller RD (1998) Avoiding pitfalls in shallow seismic reflection surveys. *Geophysics* 63(4):1213–1224
- Taner MT, Koehler F (1981) Surface consistent corrections. *Geophysics* 46:17–22
- Treadway JA, Steeples DW, Miller RD (1988) Shallow seismic study of a fault scarp near Borah Peak, Idaho. *J Geophys Res* 93:6325–6337
- Ursin B (1990) Offset-dependent geometrical spreading in a layered medium. *Geophysics* 55(4):492–496
- Widess MB (1973) How thin is a thin bed? *Geophysics* 38(6):1176–1180
- Yilmaz O (1987) *Seismic data processing*. Society of Exploration Geophysics, Tulsa
- Yilmaz O (2001) *Seismic data analysis*. Society of Exploration Geophysics, Tulsa